Available online at www.sciencedirect.com
SCIENCE DIRECT®
Journal of Solid State Chemistry 178 (2005) 511–520
JOURNAL OF SOLID STATE CHEMISTRY
www.elsevier.com/locate/jssc

Heavy metal phosphate nanophases in silica: influence of radiolysis probed via *f*-electron state properties

James V. Beitz*, C.W. Williams, K.-S. Hong, G.K. Liu

Chemistry Division, 9700 South Cass Avenue, Argonne National Laboratory, Argonne, IL 60439-4831, USA

Received 1 June 2004; received in revised form 3 September 2004; accepted 10 September 2004
Available online 11 November 2004

Abstract

We have assessed the feasibility of carrying out time- and wavelength-resolved laser-induced fluorescence measurements of radiation damage in glassy silica. The consequences of alpha decay of Es-253 in $LaPO_4$ nanophases embedded in silica were probed based on excitation of 5*f* states of Cm^{3+}, Bk^{3+}, and Es^{3+} ions. The recorded emission spectra and luminescence decays showed that alpha decay of Es-253 ejected Bk-249 decay daughter ions into the surrounding silica and created radiation damage within the $LaPO_4$ nanophases. This conclusion is consistent with predictions of an ion transport code commonly used to model ion implantation. Luminescence from the $^6D_{7/2}$ state of Cm^{3+} was used as an internal standard. Ion–ion energy transfer dominated the dynamics of the observed emitting 5*f* states and strongly influenced the intensity of observed spectra. In appropriate sample materials, laser-induced fluorescence provides a powerful method for fundamental investigation of alpha-induced radiation damage in silica.

Keywords: Radiation damage; Nanophase; *f*-element spectroscopy; Laser-induced fluorescence; Ion–ion energy transfer

1. Introduction

We have carried out an initial study designed to determine the feasibility of using laser-based techniques to fundamentally investigate radiation damage in glassy silica when that damage is due to alpha decay occurring in heavy metal phosphate nanophases that are embedded in the silica. The majority of presently used or proposed nuclear waste forms are heterogeneous in that the radioactive isotopes replace one or more types of framework metal ions [1]. The degree of heterogeneity in silica-based glass waste forms is increased further if incomplete dissolution of the loaded radioactive isotopes occurs or if precipitation creates insoluble phases, such as heavy metal phosphates, on the nano, micro or macro scales [2]. Determining the effect of heterogeneity due to nanophase inclusions on radiation damage in glasses is particularly challenging both as to sample preparation and characterization. In addition, bulk phases being considered as hosts for storage of radioisotopes are likely to contain a high defect density due to waste form processing that creates embedded defect phases whose size may range from the nano to the macro scale. For example, lanthanum-gadolinium orthophosphates powders of the monazite structure type recently have been investigated as ceramics for nuclear waste storage although densification no higher than 96% of theoretical was achieved [3].

The basis of our sample preparation method is a material termed Diphosil that is ~90% silica by dry weight. Diphosil is a chemically functionalized, highly porous silica that was created to nearly irreversibly sorb highly charged metal ions, such as trivalent lanthanide or actinide ions, from nitric acid solutions at up to 10 mol/L HNO_3 [4]. Our past studies on heavy metal ion-loaded Diphosil have shown that heavy metal phosphate nanophases form upon heating to 1373 K

*Corresponding author. Fax: +630 252 4225.
E-mail address: beitz@anl.gov (J.V. Beitz).

0022-4596/$ - see front matter © 2004 Elsevier Inc. All rights reserved.
doi:10.1016/j.jssc.2004.09.019

and holding that temperature for one hour [5]. Heating oxidizes the organic content of Diphosil to carbon dioxide and water vapor and results in a material that is ~93% silica by weight with the remainder being heavy metal ions and phosphate bonded to heavy metal ions or silica. For light to mid-series lanthanides, such as Eu^{3+}, the resulting nanophases, based on X-ray powder diffraction, are lanthanide orthophosphates of the monazite structure type whereas pore collapse produces silica is that vitreous. The heavy metal phosphate nanophases typically are 5.2 nm in diameter with a polydispersivity of 1.4 nm based on fitting small angle X-ray scattering data to a Schultz polydisperse sphere model [6].

In the case of Eu-loaded Diphosil, complex and rapid luminescence decay of the Eu^{3+} $^5D_0$ state results from facile ion–ion energy transfer attributed to the close proximity of Eu^{3+} ions in the $EuPO_4$ nanophases. However, single exponential decay at nearly the purely radiative rate of the $^5D_0$ state was observed from a sample loaded with a solution that contained La:Eu in the atom ratio 500:1 [5]. The $^5D_0$ state emission spectra in both cases consisted of rather broad lines and were the same to within experimental error. The decay rate and emission spectrum are evidence that the Eu^{3+} ions were dispersed in the $LaPO_4$ nanophases. Fully lanthanide (Ln) ion-loaded Diphosil contains four P atoms per Ln atom. Formation of $LnPO_4$ nanophases leaves residual phosphate that would be expected to react with silica to form silicophosphate. A preliminary P-31 NMR study (J. V. Beitz and J. Muntean, unpublished) on La-loaded Diphosil that had been heated to 1373 K showed the expected P-31 resonance of P atoms in lanthanum orthophosphate of the monazite structure type [7] and the resonances of P atoms in silicophosphate environments as reported in studies on phosphoric acid interaction with silica at high temperature [8].

To determine the effect of heterogeneity due to nanophase inclusions on radiation damage we created a sample that, as of the date of its preparation, contained equal concentrations of Es-253 (an alpha emitting isotope with a 20.47 day half-life), Bk-249 (a principally beta emitting isotope with a 330 day half life) and Cm-245 (an alpha emitting isotope with a 8500 year half life). Because Es-253 decays to Bk-249 that principally decays to Cf-249 (an alpha emitting isotope whose half life is 351 years), luminescence recorded shortly after sample preparation was due to Cm^{3+}, Bk^{3+} and Es^{3+} in the absence of significant radiation damage. Luminescence spectra recorded periodically throughout the decay of Es-253 included contributions from the Bk-249 present at sample preparation and Bk-249 from alpha decay of Es-253 that occurred after sample preparation. Both of these types of Bk, in turn, were decaying to Cf-249, albeit much more slowly than Es-253 decays. Cm-245 is the decay daughter of Cf-249. However, its principal role here was to serve as an internal standard, i.e., as a source of comparatively narrow band emission from an ion that does not undergoing any significant nuclear decay on the time scale of the experiment. Nuclear decay data cited above and hereafter are from the National Nuclear Data Center [9].

2. Experimental details

Diphosil, in the form of a 60–100 mesh powder, was purchased from Eichrom Technologies Inc. (Darien, IL) as "Diphonix® on silica". The composition of this material as to silica substrate, phosphorus atom content (present as a derivative of diphosphonic acid), and concentration of exchangeable protons are the same as the material synthesized by Chiarizia et al. [4]. Es-253 and Cm-245 were obtained from the Radiological Engineering Development Center at Oak Ridge National Laboratory. The as-received Es-253 was allowed to undergo one decay half-life and then was used for sample preparation without removal of the Bk-249 decay daughter or the trace level of its slowly in-growing Cf-249 progeny. A nitric acid solution was prepared that contained La^{3+}, $^{245}Cm^{3+}$, $^{249}Bk^{3+}$, and $^{253}Es^{3+}$ in the atom ratios of 0.989:0036: 0.0036:0.0036, respectively. This solution was added to dried Diphosil (28 mg) in a platinum crucible. The loading solution contained the number of metal ions needed to fill the metal ion binding sites in the Diphosil particles. The contents of the crucible were taken to dryness by heating under a dry nitrogen gas stream. The crucible was heated to 1373 K in air in a vertical tube furnace at a 1 K per minute rate of temperature rise, held at 1373 K for one hour, and then cooled quickly to ambient by terminating heating power to the furnace. The resulting free-flowing colorless powder was transferred into a 6 mm diameter fused silica tube one end of which had been drawn down to a 1 mm diameter. The sample tube was evacuated, backfilled with a few Torr of He gas (for thermal contact), and flame-sealed. In reflected light, the powder in the sample tube appeared white due to light scattering. In the absence of any illumination, the sample powder emitted orange-red light visible to the eye, principally due to radiolysis from decay of Es-253 and subsequent energy transfer to Cm^{3+}. Using the same preparative method, a sample that contained La:Cm-245 in the atom ratio 0.997:0.003 in Diphosil was prepared. That sample emitted no light discernible by a dark-adapted eye.

Unless otherwise stated, the 355 nm third harmonic of a Q-switched Nd:YAG laser was the excitation source for time- and wavelength-resolved laser-induced fluorescence studies. Lenses collected luminescence from the sample and directed it through long pass optical filters into a one meter monochromator. Computer-interfaced

boxcar detectors recorded the luminescence intensity of the sample at a particular wavelength in a selected time window following pulsed laser excitation. Luminescence was detected using a cooled Ga:As photocathode photomultiplier that was located at the exit slit of the monochromator. Luminescence at longer than 850 nm was detected using a cooled photomultiplier with an *S*-1 response photocathode. The sample was placed into a heat exchange gas cryostat for experiments at cryogenic temperature. The luminescence spectrum of the sample was recorded using various gate delays and widths to aid in assigning observed bands to particular emitting states. This data collection process was repeated periodically over several months to assess the consequences of increasing radiation damage and formation of decay daughter nuclei.

3. Experimental results

Here and throughout this paper the term symbols used for particular 5*f* states are those listed by Carnall [10]. One of the initially recorded luminescence spectra from the $La_{0.989}Cm_{0.0036}Bk_{0.0036}Es_{0.0036}$ in Diphosil sample that had been heated to 1373 K (hereafter, La + Cm + Bk + Es sample) are shown in Fig. 1a. The emission peaking at 660 nm in Fig. 1a is assigned to the Bk^{3+} $^7F_6 \rightarrow {}^7F_6$ transition based on the observed wavelength and its comparatively short lifetime [11,12]. Based on the known energy level structure of Cm^{3+}, the band peaking at 603.1 nm is assigned as arising from the Cm^{3+} $^6D_{7/2} \rightarrow {}^8S_{7/2}$ transition [11]. This was confirmed by using a longer gate delay (see Fig. 1b) and by the emission spectrum of the $La_{0.997}Cm_{0.003}$ in Diphosil sample that had been heated to 1373 K (not shown). The initial emission spectra of Cm^{3+} were little influenced by sample temperature, from ambient to cryogenic, aside from anti-Stokes vibronic bands whose intensity increased with increasing sample temperature (compare Fig. 1b and Fig. 2). A series of broad emission bands (not shown), peaking initially at 1036 nm and extending to 1120 nm (limited by decreasing sensitivity of the detection system at increasing wavelength) were observed and are attributed to the Es^{3+} $^5F_5 \rightarrow {}^5I_8$ transition [11].

As noted above, luminescence spectra were recorded periodically over the course of the decay of Es-253. Fig. 2 shows a comparison of Cm^{3+} emission spectra recorded 1 day and 107 days after sample preparation. Insight into some of the factors influencing observed luminescence intensity was gained by multiplying the intensity values for each spectrum by a constant to give approximately equal peak intensity for the Cm^{3+} $^6D_{7/2} \rightarrow {}^8S_{7/2}$ transition and then offsetting the resulting spectra vertically for clarity (see Fig. 3). It is evident that the Cm^{3+} emission transition broadens and, to a smaller

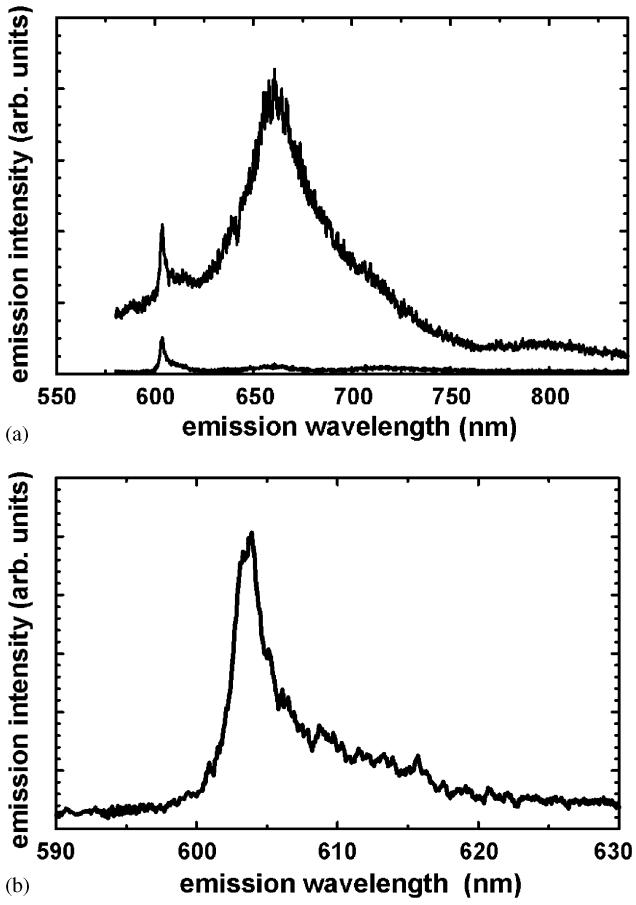

Fig. 1. Emission spectra recorded at 2.6 K following pulsed excitation at 355 nm of the La + Cm + Bk + Es sample 2 days after sample preparation. The most prominent peak in the upper curve of panel a is due to the $^7F_6 \rightarrow {}^7F_6$ transition of Bk^{3+}. Panel (a) boxcar gate settings were 10 μs delay and 5 μs width for the upper curve and 120 μs delay and 15 μs width for the lower curve. Panel (b) shows an enlargement of the Cm^{3+} $^6D_{7/2} \rightarrow {}^8S_{7/2}$ transition region of the lower curve in panel a.

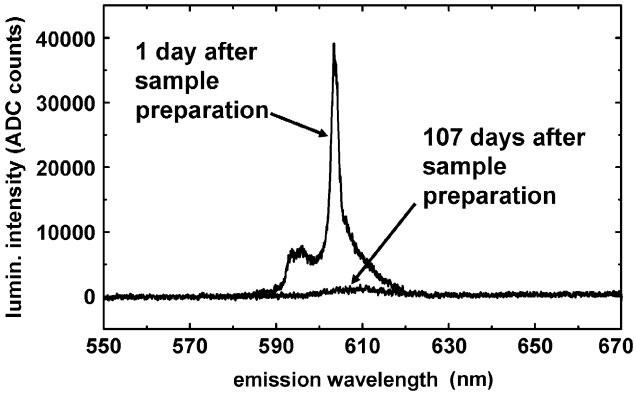

Fig. 2. Comparison of emission spectra of the Cm^{3+} $^6D_{7/2} \rightarrow {}^8S_{7/2}$ transition that were recorded at 295 K following pulsed excitation at 355 nm of the La + Cm + Bk + Es sample at 1 day and 107 days after sample preparation. Boxcar gate delay and width were 100 and 15 μs, respectively.

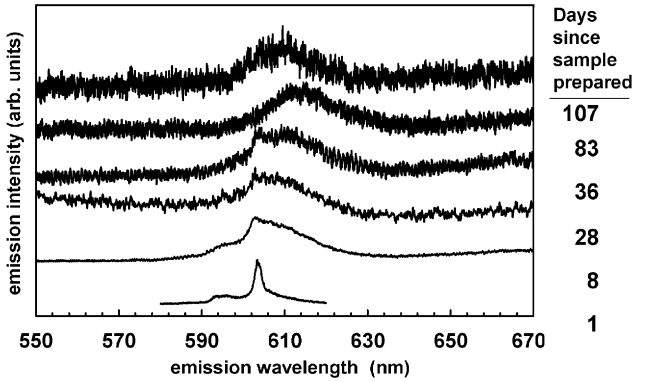

Fig. 3. Observed emission spectra in the Cm^{3+} $^6D_{7/2} \rightarrow {}^8S_{7/2}$ transition region of the La + Cm + Bk + Es sample, following 355 nm excitation, recorded at the stated time following sample preparation. Intensities were normalized to give approximately equal peak amplitude for the Cm^{3+} transition that initially peaked at 603.1 nm. Spectra offset vertically for clarity. Boxcar gate delay and width were 100 and 15 μs, respectively.

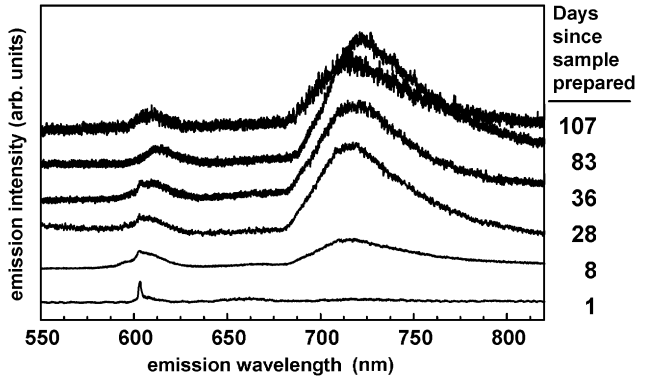

Fig. 4. Observed emission spectra of the La + Cm + Bk + Es sample, following 355 nm excitation, recorded at the stated time following sample preparation. Intensities were normalized to give approximately equal peak amplitudes for the Cm^{3+} $^6D_{7/2} \rightarrow {}^8S_{7/2}$ transition. Spectra offset vertically for clarity. Boxcar gate delay and width were 100 and 15 μs, respectively.

degree, shifts over the time period studied which corresponds to more than five half lives of the decay of Es-253. Fig. 4 (which includes the spectra shown in Fig. 3) compares emission spectra recorded over the same time interval and a broader spectral range. It is evident that a new emission band, peaking at 715 nm, grew in whose intensity first increased relative to that of the Cm^{3+} band and then began to decrease. The 660 nm band of Bk^{3+} is nearly absent in Fig. 4 due to the comparatively long boxcar gate delay used to record those spectra. The 660 nm band is evident in the spectra compared in Fig. 5 which also have been scaled to the Cm^{3+} band and offset. The spectra in Fig. 5, recorded with a shorter boxcar gate delay and narrower gate width, show the 660 nm emission band of Bk^{3+} and provide evidence that its intensity, relative that of

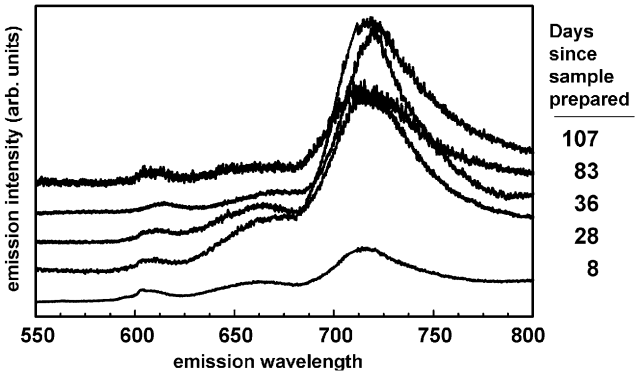

Fig. 5. Observed emission spectra of the La + Cm + Bk + Es sample, following 355 nm excitation, recorded at the stated time following sample preparation. Intensities were normalized to give equal peak amplitude for the Cm^{3+} $^6D_{7/2} \rightarrow {}^8S_{7/2}$ transition that initially peaked at 603.1 nm. Spectra offset vertically for clarity. Boxcar gate width was 5 μs and boxcar gate delays were 10 μs or 15 μs.

Cm^{3+}, changed only modestly, in comparison with the new 715 nm band. From the signal-to-noise ratio, it is also evident that luminescence intensity decreased for the 603 nm Cm^{3+} $^6D_{7/2} \rightarrow {}^8S_{7/2}$ band, the 660 nm Bk^{3+} $^7F_6 \rightarrow {}^7F_6$ band that was present immediately after sample preparation and the new 715 nm band which is the only emission band whose intensity grew in, relative to the intensity of the Cm^{3+} emission band. For reasons discussed below, the 715 nm band is attributed to Bk that resulted from alpha decay of Es-253 in the sample after preparation.

4. Discussion

Past luminescence studies on the influence of alpha radiolysis on the 5*f* emission bands of Cm^{3+} in bulk $LuPO_4$ showed that an average atom displacement of 0.002 nm resulted in a 20 cm^{-1} inhomogeneous line width for the $^6D_{7/2} \rightarrow {}^8S_{7/2}$ transition of Cm^{3+} [13]. For this reason, it is not unexpected that alpha radiolysis in the La + Cm + Bk + Es sample would result in broadening of the Cm^{3+} 5*f* transitions or the 5*f* transitions of the other actinide ions that were present initially or grow in. The rapid loss of luminescence intensity from the initially present Cm^{3+} and Bk^{3+} ions as Es-253 decay occurred, however, does require explanation as does the appearance of an in-growing band of substantial spectral width whose luminescence intensity was much less influenced by Es-253 decay.

The starting point for explaining both of these observations is consideration of the time evolution of isotopic species due to nuclear decay processes in the La + Cm + Bk + Es sample. See Fig. 6. Over the time span of our luminescence observations, all but about 1.5% of the initially present Es-253 underwent alpha decay. A significant fraction of the initially present

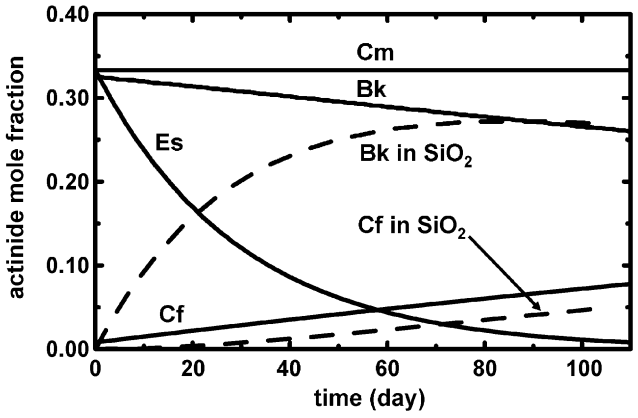

Fig. 6. Calculated mole fraction of the actinide content of the La + Cm + Bk + Es sample as a function of time following sample preparation. The sample contained two types of Bk-249: Bk-249 that was present at sample preparation and Bk-249 from decay of Es-253 after sample preparation. For reasons stated in the text, the latter is labeled "Bk in SiO_2" and its progeny is labeled "Cf in SiO_2".

Bk-249, and a lesser fraction of the Bk-249 that grew in after sample preparation, decayed by beta emission to Cf-249 over our time span . A very small fraction (1.4×10^{-5}) of Bk-249 decay is alpha emission that, due to the 2.05 h half-life of Am-245, quickly results in formation of Cm-245. Due to its infrequency, this decay path is not included Fig. 6.

Consideration of the 5*f* state energy level structure of the transamericium ions Cm^{3+}, Bk^{3+}, Cf^{3+}, and Es^{3+} is essential for interpreting our observations. The relevant portion of the 5*f* state energy level structure of trivalent actinide ions in $LaCl_3$, from the work of Carnall [11], is shown in Fig. 7. The primary emitting transition that we observed in our studies is shown as a downward pointing arrow in Fig. 7.

4.1. Luminescence decay

Although 5*f* state actinide ion–ion energy transfer has not been as extensively studied as has that involving the 4*f* states of lanthanide ions, it is known that 5*f* electron states behave similarly to the 4*f* electron states of lanthanide ions [14]. Hence it is likely that the predominant ion–ion energy transfer processes in the La + Cm + Bk + Es sample occurred via the Forster-Dexter mechanism which for 4*f* states is known to provide measurable probability for energy transfer between lanthanide ions over distances up to about 1 nm. Prior to significant radiation damage occurring, luminescence from the $^6D_{7/2}$ state of Cm^{3+} in the La + Cm + Bk + Es sample was well fit (see Fig. 8) by the equation

$$I(t) = I_0 \exp\left(-\frac{t}{\tau} - 2C\left(\frac{t}{\tau_r}\right)^{1/2}\right) \quad C = \frac{2}{3}\pi^{2/3} n_q R_0^3, \qquad (1)$$

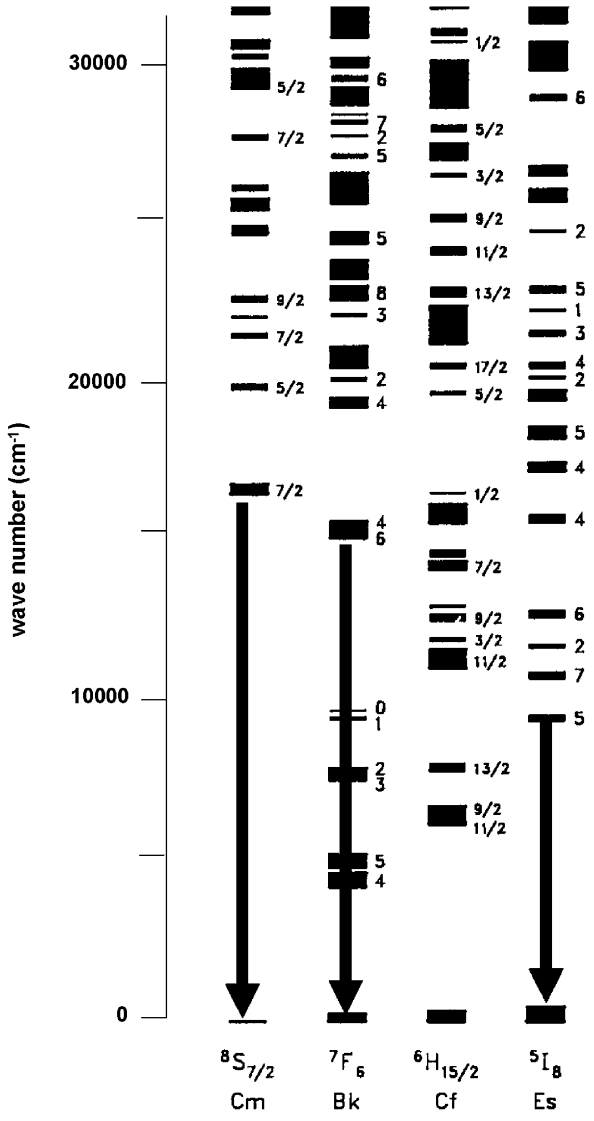

Fig. 7. The 5*f* state energy level structure of trivalent Cm, Bk, Cf, and Es ions in $LaCl_3$ from the work of Carnall [11].

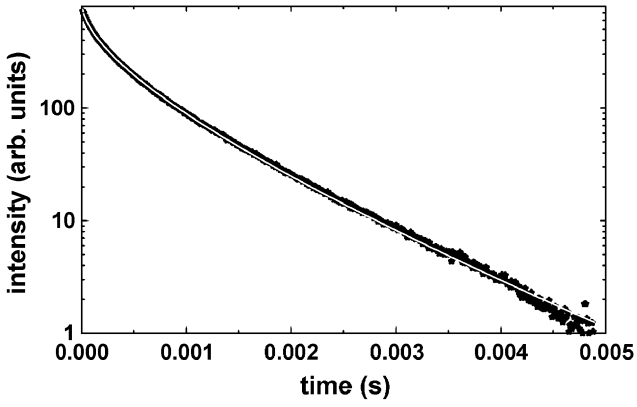

Fig. 8. Observed 603 nm luminescence decay of Cm^{3+} following 355 nm excitation of the La + Cm + Bk + Es sample at 295 K one day after sample preparation (symbols) and a nonlinear least squares fit of those data to Eq. (1) that resulted in the values $C = 1.19$ and $\tau_r = 1.74$ ms (white line).

where $I(t)$ is the observed luminescence intensity at time t, τ_r is the intrinsic decay time of the excited donor ion, n_q is the concentration of acceptor (quenching) ions, and $R_0 = \tau_r R^6 W(R)$, where $W(R)$ is the transition probability for energy transfer and R is the distance separating the donor and acceptor ions. The above equation, due to the work of Watts [15], assumes dipole–dipole interaction, a statistical distribution of both donor and acceptor ions, and the absence of energy migration among the donor ions. It has been used to interpret the 4*f* state luminescence decays observed from free standing nanophases of $La_{0.95}Eu_{0.05}PO_4$ and $Ce_{0.85}Tb_{0.15}PO_4$ of 5 nm mean diameter [16]. The fit values of τ_r and C for the La + Cm + Bk + Es sample at 295 K one day after its preparation were 1.74 ms and 1.19, respectively. The fit value of τ_r agrees well with the calculated 1.3 ms purely radiative lifetime of aquated Cm^{3+} [17]. For comparison, the fit values of τ_r and C for luminescence from the $^5D_4$ state of Tb^{3+} in $Ce_{0.85}Tb_{0.15}PO_4$ were 3.2 ms and 1.28, respectively [16].

Subject to the condition that the luminescence quantum yield, ϕ, of the emitting state is equal to unity in the absence of ion–ion energy transfer, integration of Eq. (1) results in the following relationship [16].

$$\phi = 1 - \pi^{1/2} C \exp(C^2) erfc(C). \quad (2)$$

Due to the large energy gap between the $^6D_{7/2}$ state of Cm^{3+} and its next lower lying state, it would be expected that the quantum yield of the $^6D_{7/2}$ state would be unity in the absence of ion–ion energy transfer. The fit value of C for the data shown in Fig. 8 results in a calculated quantum yield of 0.2, using Eq. (2), for the $^6D_{7/2}$ state of Cm^{3+} in the La + Cm + Bk + Es sample one day after preparation. A calculated quantum yield significantly less than unity is an indication of the importance of ion–ion energy transfer and is evidence for the close proximity of acceptor ions to Cm^{3+} prior to the accumulation of any significant amount of radiation damage.

The luminescence decay of the 715 nm emission band was complex and typical of decays observed from multiphonon decay of 4*f*-states of lanthanide ions embedded in glasses when there are multiple ion sites that exhibit site-dependent nonradiative decay rates [18]. Fig. 9 shows a plot of the decay time per e-fold loss of luminescence intensity at 715 nm, following pulsed 355 nm excitation, for the La + Cm + Bk + Es sample as a function of temperature for data recorded 36 days after sample preparation.

4.2. Energy transfer

From Fig. 7, it is evident that Cm^{3+} in its $^6D_{7/2}$ state near 17,000 cm^{-1} can transfer energy to Bk^{3+}, Cf^{3+}, and Es^{3+} with probabilities that depend on the local environment of each ion (crystal field splitting) and the

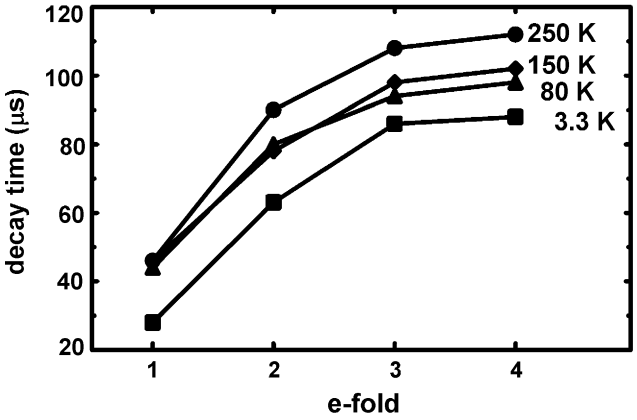

Fig. 9. Observed time per e-fold decay as a function of the number of e-fold decays of luminescence at 715 nm following 355 nm excitation of the La + Cm + Bk + Es sample at the temperature shown at 36 days after sample preparation.

distance separating the ions being considered. In our case, the local environment changed with time due to radiation damage primarily arising from decay of Es-253. In addition, a 5.2 nm diameter $LaPO_4$ spherical nanophase contains approximately 1014 La ions. For the La + Cm + Bk + Es sample, this means that each nanophase would be expected to initially have contained, on average, 3 to 4 Cm^{3+} ions, 3 to 4 Bk^{3+} ions, and 3 to 4 Es^{3+} ions. The Es-related channel of ion–ion transfer of 5*f* state energy naturally diminished as Es decay occurred.

Insight into the extent to which in-growing Bk could quench the $^6D_{7/2}$ state of Cm^{3+} was gained by carrying out calculations using the TRIM computer code contained in the SRIM-2003 package of programs created by Zeigler and coworkers [see http://www.srim.org/]. Atom displacements and ion range were calculated for the case of 106 keV uranium ions (simulating a recoiling Bk-249 nucleus following Es-253 alpha decay). The uranium ions were assumed to be incident on a layered planar structure that consisted of a 2.5 nm thick layer of $LaPO_4$, then a 1.7 nm thick layer of silicophosphate (assumed to consist of SiP_2O_7) and finally a 100 μm thick layer of SiO_2 glass. Atom displacements due to incident 6.6 MeV helium ions (simulating the alpha particles from Es-253 decay) were calculated as well. The calculated number of displaced atoms per nm of depth into the layered structure for incident 106 keV uranium ions is shown in Fig. 10. The calculated range of the U ions (46.3 nm with 10.1 nm straggle) significantly exceeds the 17 nm average separation distance of the 5.2 nm diameter $LaPO_4$ nanophases in the La + Cm + Bk + Es sample. This means that Bk that grew in after sample preparation was ejected from its parent $LaPO_4$ nanophase and would, in most cases, damage one or more of the other surrounding $LaPO_4$ nanophases before coming to rest, in the large majority

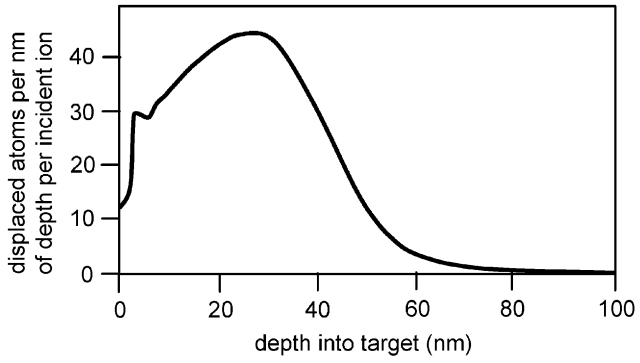

Fig. 10. Calculated number of displaced atoms as a function of depth into a layered planar structure (2.5 nm of $LaPO_4$, then 1.7 nm of SiP_2O_7, and finally 100 μm of glassy SiO_2) for incident 106 keV U ions.

of cases, in a (damaged) silica local environment. Due to increased donor-acceptor distance and considering a $1/R^6$ distance dependence for dipole–dipole energy transfer, 5*f* states of in-growing Bk ions would be much less susceptible to nonradiative decay due to ion–ion energy transfer than would be the actinide ions that remained within the $LaPO_4$ nanophases. Conversely, in-growing Bk^{3+} ions would have little influence on the nonradiative decay of any of the actinide ions in the $LaPO_4$ nanophases.

The total number of atom displacements calculated using TRIM per simulated Es-253 decay was 1920. Taking into consideration the Es-253 content of the La + Cm + Bk + Es sample, 2% of the atoms in our sample underwent an atom displacement event over the course of our studies. Based on ORIGEN calculations [19], if the uranium through curium isotopes contained in 33,000MW-day burn up spent fuel from a light water reactor after 10 years storage were sorbed into Diphosil that then was heated to 1373 K, cooled to ambient and stored, it would take ~3000 year for the same number of alpha decay events to occur per unit weight of the stored material as we achieved in our La + Cm + Bk + Es sample.

Based on the TRIM calculations, the local environment around the initially present Bk ions became more disordered due to radiation damage of the $LaPO_4$ nanophases. In addition, the initially present Bk ions (those in the $LaPO_4$ nanophases), in part, underwent beta decay to Cf-249. Beta decay produces little recoil of the decay daughter Cf-249. Overall, one would expect increased local disorder for the Cm^{3+}, Bk^{3+}, Cf^{3+} and Es^{3+} ions in the $LaPO_4$ nanophases as Es-253 alpha decay proceeded with little additional radiation damage due to decay of Bk-249. To the extent that increasing local disorder improved ion–ion transfer by broadening optical transitions and that increased spectral overlap between donor and acceptor ions, then alpha radiolysis increased ion–ion energy transfer in our La + Cm + Bk + Es sample.

If, as one would expect based on Fig. 7 and the reported absorption spectra of aquated Bk^{3+} and Cf^{3+} ions [17], Cf^{3+} provides both better spectral overlap and reduced energy mismatch than does Bk^{3+} for transfer of energy from the $^6D_{7/2}$ state of Cm^{3+}, then in-growth of Cf-249 in the $LaPO_4$ nanophases would result in enhanced nonradiative decay of Cm^{3+}. In the case of the Bk ions initially present in the $LaPO_4$ nanophases, 5*f* state ion–ion energy transfer presumably occurred originally to Es^{3+} and subsequently to Cf^{3+}. The Bk^{3+} that grew in after sample preparation resided primarily in a silica local environment that became more disordered as additional Es-253 decay occurred. Presumably such increased disorder opened new nonradiative decay paths, not involving ion–ion energy transfer, for such Bk^{3+} ions and, in consequence, diminished the intensity of 5f state luminescence from those ions.

The 715 nm band was the only emission band observed to grow in, relative to that of the 603 nm band of Cm^{3+}, with decay of Es-253 which is evidence that the 715 nm band was due to Bk ions that were the decay daughters of the Es^{3+} in the $LaPO_4$ nanophases. The 715 nm band was unusually broad and not strongly influenced as to width by accumulation of radiation damage or temperature. The breadth of the band and the lack of significant temperature dependence are consistent with the decay daughter Bk having been ejected from $LaPO_4$ nanophases and coming to rest in the surrounding glassy silica in a wide variety of local environments. Its luminescence decay was complex and became faster with decreasing temperature. Complex luminescence decay via multiphonon emission is typically observed from f-state ions in glass samples due to a broad distribution of local environments [18]. The observation of more rapid luminescence decay with decreasing sample temperature is unusual and seems likely to reflect the consequences of radiation damage in the immediate surroundings of the Bk ions.

4.3. Valence of Bk from Es decays after sample preparation

The oxidation state of the Bk ions that emit at 715 nm is most simply assigned as trivalent although the difference of 1165 cm^{-1} between the 660 and 715 nm peaks requires that there be a large shift in the center gravity of the emitting $^7F_6$ multiplet of Bk^{3+} when the ion's local environment changes from that in the $LaPO_4$ nanophases to that in radiation-damaged glassy silica. No studies on the 5*f* state energies of Bk^{3+} in glassy silica have been published although Assefa and co-workers have reported emission bands peaking at 648 and 742 nm from Bk^{3+} in borosilicate glass [20]. They did not, however, assign either of these bands as arising from a particular 5*f* emitting state or states. If the 715 nm emission band in our studies is due to Bk^{3+},

then the local environment of those Bk ions would have to have been altered significantly, presumably due to radiation damage, to account for the large shift in energy of the emitting multiplet relative to 5*f* state energies of Bk^{3+} in $LaCl_3$. Assignment of our observed 715 nm band to the $^6D_{7/2}$–$^8S_{7/2}$ transition of Bk^{4+} is an alternative. However, because the longest wavelength purely electronic emission from the $^6D_{7/2}$ state of Bk^{4+} in CeF_4 occurs at 612.9 nm [21], this would require an even larger shift in the energy of the emitting multiplet. This seems unlikely if the crystal field strength of *f*-element ions in glassy silica is comparable to that of trivalent *f*-elements ions when aquated or doped into $LaCl_3$ which are weak crystal field cases.

In a study on Tb ion implantation into a 200 nm thick layer of glassy silica, luminescence from Tb^{3+} ions after annealing was measured. The authors concluded that the observed 4*f*–4*f* transition energies of the Tb^{3+} ions differed little (0–5.8 nm) from those of aquated Tb^{3+} ions [22]. We conclude that the 715 nm emission band in our studies is due to Bk from decay of Es-253 after sample preparation and that such Bk probably is trivalent although we cannot rule out the possibility that it is tetravalent on unusual sites in radiation damaged glassy silica.

4.4. Reversal of radiation damage

In our discussion, to this point, we have not considered the possibility that the passage of energetic charged particles through our sample material could reverse radiation damage previously caused by other such particles. Evidence that structural radiation damage can be reversed due to incidence of 80–200 keV electrons on a film of amorphous $LaPO_4$ was reported by Meldrum et al. [23]. Over the course of our laser-excitation experiments, our only observations suggestive of a possible healing of radiation damage due to additional nuclear decay events were reversal, after most of the Es-253 had decayed, of the trend in which the center of gravity of the Cm^{3+} $^6D_{7/2}\rightarrow{}^8S_{7/2}$ emission band and the 715 nm emission band (due to in-growing Bk) initially shifted toward longer wavelength (see Figs 3–5). Meldrum and coworkers also reported that at 308 K or higher sample temperature amorphization (loss of crystallinity) did not occur when high energy Kr^+ ions were incident on single crystal $LaPO_4$ although amorphization did occur at lower sample temperature under the same irradiation conditions [24]. The La + Cm + Bk + Es sample that we investigated was held at (295 ± 2) K aside from some brief periods when laser excitation studies were carried out at cryogenic temperatures. As is evident in Figs. 2–4, this sample underwent net radiation damage, principally due to alpha decay of Es-253, that was easily observable using laser excitation methods.

Due to the nanophase character of the $LaPO_4$ in our sample, one might have expected more facile ion movement, and consequent greater difficulty in creating net radiation damage, at a given temperature, in comparison with bulk single crystal $LaPO_4$. However, it should be noted that the source of radiation damage differed in the present work and that of Meldrum et al. as did the methods used to assess radiation damage.

4.5. Silica defect luminescence and prior studies of Es-doped glasses

In our studies, radiation damage occurred both within $LaPO_4$ nanophases and the glassy silica in which such nanophases were embedded. It is known that many defects in silica, including some of those induced by radiation damage, luminescence following ultraviolet excitation [25,26]. In addition, Assefa and Hare studied self- and photo-induced luminescence of borosilicate glass that contained 1% Es-253 by weight [27]. They attributed all of the luminescence that they observed to defect centers created by radiation damage from alpha decay of Es-253. Self-luminescence spectra starting at 3 days and extending to 90 days after sample preparation were reported. Self-luminescence peaks at 455, 650 and 730 nm were observed with the 650 and 730 nm bands becoming more intense with increasing time after sample preparation whereas the 455 nm peak systematically decreased in intensity. Luminescence bands peaking at 650 and 730 nm were observed following 488 nm photoexcitation. It is natural, therefore, to consider whether or not radiation-induced defects in glassy silica contributed significantly to the luminescence that we observed following 355 nm excitation in our studies.

Sukarai investigated the tendency for formation of a 689 nm luminescing defect (145 nm FWHM spectral width), attributed to oxygen deficiency, in glassy silica as a function of oxygen partial pressure during glass melting and the hydroxide and chloride ion contents of the glass [28]. Melting in a 1% oxygen atmosphere produced the 689 nm luminescing defect whereas gamma irradiation was required to produce it in samples melted at higher oxygen partial pressure. Observable EPR signals and photoluminescence from the defect were lost for glass that had been melted under 15% oxygen and then gamma irradiated.

Our La + Cm + Bk + Es sample and Assefa and Haire's Es-borosilicate sample were heated in air (20.9% nominal oxygen content) in a platinum crucible which presumably should have strongly suppressed the formation of the 689 nm luminescing structural defect in the glass phases. A luminescing defect, variously reported to peak at 653–670 nm, is reported to occur in silica that contains a surplus of oxygen [29]. That defect exhibits complex luminescence decays (lifetimes ranging from 10 μs to 5 ms) depending on glass

composition and processing variables but its formation requires unusual conditions (such as heating silica in pure O_2 gas to 1473 K or irradiation of silica in the presence of ozone). Based on our sample preparation conditions, formation of an oxygen surplus defect is unlikely in our sample. In addition, because our 660 nm emission band was present in the first spectra we recorded (1 day after sample preparation) and decreased in intensity as Es-253 decayed, it is unlikely that any significant number of oxygen surplus defects were created in the silica phase of our sample material by alpha decay of Es-253. We note that the 650 nm and 730 nm emission bands from ^{253}Es-borosilicate glass that were attributed to silica defects by Assefa and Haire [27] are little different in wavelength and exhibited similar laser power dependence to the 652 and 742 nm emission bands of Bk^{3+} in borosilicate glass of the same nominal chemical composition that were reported earlier by Assefa et al. [20].

In summary, the silica-related defects in our La + Cm + Bk + Es sample likely made little contribution to our recorded luminescence spectra and lifetimes. The conclusion of Assefa and Haire that luminescence from silica-related defects gave rise to all of the self- and photo-induced luminescence from their ^{253}Es-borosilicate glass sample should be re-examined in light of our present study and the earlier study of Assefa et al. on the luminescence of Bk^{3+} in borosilicate glass because both of these studies suggest that the red luminescence bands from ^{253}Es-borosilicate glass were due, in large part, if not completely, to emission from Bk ions.

5. Conclusions

Our studies have shown the feasibility of using time- and wavelength-resolved laser-induced fluorescence techniques to fundamentally investigate radiation damage in glassy silica when that damage is due to alpha decay that occurs in heavy metal phosphate nanophases embedded in the silica. Using Cm^{3+} as an internal luminescence standard, the effects of alpha radiolysis on the spectra of selected excited 5*f* states of Cm^{3+}, Bk^{3+}, and Es^{3+} ions were determined and qualitatively interpreted. The luminescence decay of $^6D_{7/2}$ state of Cm^{3+} was shown to be dominated by ion–ion energy transfer to surrounding actinide ions in the $LaPO_4$ nanophases. Changes in the emission of spectra and 5*f* state decay dynamics of Bk ions that resulted from the decay of Es-253 after sample preparation confirmed the presence of Es^{3+} in the $LaPO_4$ nanophases that formed and became embedded in vitreous silica during sample preparation. The spectra and excited state dynamics that we observed are in agreement with predictions as to heavy ion recoil distances, following alpha decay, made by an ion transport code commonly used to model ion implantation in the semiconductor industry.

Acknowledgments

The lifelong research of W. T. Carnall on the energy level structure of *f*-element ions provided the essential basis for understanding the spectra and energy transfer pathways investigated in our present studies. This work was performed under the auspices of the Office of Basic Energy Sciences (OBES), Office of Science, and the Nuclear Energy Research Initiative, US Department of Energy under Contract W-31-109-Eng-38. The authors are indebted to the OBES for the use of Cm-245 and Es-253, distributed through the Transuranium Element Program of the Oak Ridge National Laboratory.

References

[1] M.-S. Yim, K.L. Murty, JOM 52 (2000) 26–29.
[2] J.W. William, R.C. Ewing, C.A. Angell, G.W. Arnold, A.N. Cormack, J.M. Delaye, D.L. Griscom, L.W. Hobbs, A. Navrotsky, D.L. Price, A.M. Stoneham, M.C. Weinberg, J. Mater. Res. 12 (1997) 1946–1978.
[3] O. Terra, N. Clavier, N. Dacheux, R. Podor, New J. Chem. 27 (2003) 957–967.
[4] R. Chiarizia, E.P. Horwitz, K.A. D'Arcy, S.D. Alexandratos, A.W. Trochimczuk, Solvent Extr. Ion Exc. 14 (1996) 1077–1100.
[5] J.V. Beitz, C.W. Williams, Solvent Extr. Ion Exc. 19 (2001) 699–723.
[6] J.V. Beitz, S. Skanthakumar, S. Seifert, P. Thiyagarajan, Mater. Res. Soc. Symp. Proc. 802 (2004) 125–130.
[7] Y. Guo, P. Woznicki, A. Barkatt, E.E. Saad, I.G. Talmy, J. Mater. Res. 11 (1996) 639–649.
[8] N.J. Clayden, S. Esposito, P. Pernice, A. Aronne, J. Mater. Chem. 11 (2001) 936–943.
[9] National Nuclear Data Center, Upton, NY (www.nndc.bnl.gov), May 23, 2004 database.
[10] W.T. Carnall, A Systematic Interpretation of the Spectra of Trivalent Actinide Chlorides in D3 h Site Symmetry, Argonne National Laboratory Report, ANL-89/39, 1989, p. 289.
[11] W.T. Carnall, J. Chem. Phys. 96 (1992) 8713–8726.
[12] W.T. Carnall, J.V. Beitz, H. Crosswhite, J. Chem. Phys. 80 (1984) 2301–2308.
[13] G.K. Liu, V.V. Zhorin, S.T. Li, J.V. Beitz, J. Chem. Phys. 112 (2000) 373–382.
[14] G.K. Liu, J.V. Beitz, Phys. Rev. B: Cond. Matter Mater. Phys. 41 (1990) 6201–6212.
[15] R.K. Watts, in: B. Di Bartolo (Ed.), Optical Properties of Ions in Solids, Plenum Press, New York, 1975, pp. 307–336.
[16] K. Riwotzki, H. Meyssamy, A. Kornowski, M. Haase, J. Phys. Chem. B 104 (2000) 2824–2828.
[17] J.V. Beitz, in: K.A. Gschneidner, L. Eyring, G.R. Choppin, G.H. Lander (Eds.), Handbook on the Physics and Chemistry of the Rare Earths, Vol. 18, North-Holland, Amsterdam, 1994, pp. 159–195.
[18] C. Brecher, L.A. Riseberg, M.J. Weber, Phys. Rev. B: Cond. Matter Mater. Phys. 18 (1978) 5799–5811.
[19] M.J. Bell, ORIGEN—The ORNL isotope and depletion code, Oak Ridge National Laboratory, ORNL-4628, 1973, p. 144.

[20] Z. Assefa, R.G. Haire, N.A. Stump, J. Alloys Compd. 271–273 (1998) 854–858.
[21] G.K. Liu, W.T. Carnall, G. Jursich, C.W. Williams, J. Chem. Phys. 101 (1994) 8277–8289.
[22] H. Amekura, A. Eckau, R. Carius, C. Buchal, J. Appl. Phys. 84 (1998) 3867–3871.
[23] A. Meldrum, L.A. Boatner, R.C. Ewing, Mater. Res. Soc. Symp. Proc. 439 (1997) 697–702.
[24] A. Meldrum, L.A. Boatner, R.C. Ewing, Mineral. Mag. 64 (2000) 185–194.
[25] E. Dooryhee, J.P. Duraud, R.A.B. Devine, in: R.A.B. Devine, J.-P. Duraud, E. Dooryhee (Eds.), Structure and Imperfections in Amorphous and Crystalline Silicon Dioxide, Wiley, Chichester, 2000, pp. 349–421.
[26] L. Skuja, in: G. Pacchioni, L. Skuja, D.L. Griscom (Eds.), Defects in SiO_2 and Related Dielectrics: Science and Technology, Kluwer Academic Publishers, Dordrecht, 2000, pp. 73–116.
[27] Z. Assefa, R.G. Haire, ACS Symp. Ser. 778 (2001) 329–341.
[28] Y. Sakurai, Jpn. J. Appl. Phys. 39 (2000) 496–500.
[29] Y. Sakurai, J. Non-Cryst. Solids 316 (2003) 389–392.